RSC Advances

PAPER

View Article Online
View Journal | View Issue

Open Access Article. Published on 21 January 2022. Downloaded on 1/21/2026 12:12:41 AM.
This article is licensed under a Creative Commons Attribution-NonCommercial 3.0 Unported Licence.

Check for updates

Cite this: *RSC Adv.*, 2022, **12**, 2947

A novel L-histidine based ionic liquid (LHIL) as an efficient corrosion inhibitor for mild steel†

Jing Wang,[a] Chengbao Liu[b] and Bei Qian*[c]

Received 11th November 2021
Accepted 14th January 2022

DOI: 10.1039/d1ra08275b

rsc.li/rsc-advances

A novel L-histidine based ionic liquid (LHIL) was developed and successfully synthesized. Its structure was confirmed by Fourier-transform infrared spectroscopy, UV-vis spectroscopy, X-ray photoelectron spectroscopy, ^{1}H-NMR and high-resolution mass spectrometry. The outstanding corrosion inhibition effect of the LHIL on mild steel in 1 M hydrochloric acid was thoroughly evaluated by Tafel plots, electrochemical impedance spectroscopy, and localized electrochemical strategies. The results revealed that the corrosion of mild steel was effectively suppressed by the adsorption of LHIL on its surface, and the best inhibition efficiency reached 98.8%. The adsorption behavior of LHIL on steel obeyed the Langmuir adsorption isotherm, which involved both chemisorption and physisorption. Theoretical calculations indicated the strong chemisorption of LHIL on steel, as proved by the low energy gap (ΔE = 0.0522 eV) and high binding energy ($E_{binding}$ = 303.47 kcal mol^{-1}), which clearly confirmed the effectiveness of LHIL for steel protection.

1. Introduction

Acid cleaning is an effective way to remove the scale and rust generated in the inner surface of pipeline installations, and can prevent potential risks.[1,2] However, the metallic structures are highly damaged by corrosive acids during the cleaning process.[3–5] The usage of corrosion inhibitors is a practical way to inhibit the corrosion damage owing to its convenience, high efficiency, and low cost properties.[6–10] Organic substances with heteroatoms (like nitrogen, oxygen, phosphorus and so on), multiple bonds, and polar groups have been extensively studied as inhibitors to protect metal from degradation.[11–13] The protection mechanism of corrosion inhibitors relies on the validity of the adsorption film, which can block the contact between the aggressive species and metal substrate.[14–17] Heavy ions or salts such as chromate have also been applied as corrosion inhibitors.[18,19] Although they have an ideal inhibition effect, their usage was restricted by the high toxicity in water resources. Therefore, the development of green and sustainable inhibitors is in great demand.

Ionic liquid is a special kind of liquid that composes of a specific inorganic anion and organic cation (ammonium,[20–22] pyridinium[23–25] and imidazolium[26–28]). The ionic liquid can be used as corrosion inhibitor because of its non-volatility, superior solubility, and minor toxicity.[29,30] Due to their unique structure, imidazole based ionic liquids have been extensively studied for anticorrosion. It has been reported that the 1-allyl-3-octylimidazolium bromide had higher inhibition efficiency for steel compared with 1-octyl-3-methylimidazolium bromide, ascribing to the strong electron-donating ability of allyl.[28] The relationship between inhibition efficiency of imidazole based ionic liquids and the side chain length has been investigated.[27] The presence of long alkyl chains in imidazolium ring facilitates the chemical interaction between cations and metal surface.[14] Our previous work indicated that the *N*-(3-aminopropyl)-imidazole ionic liquid could effectively enhance the dispersibility of graphene in resin matrix and endowed the graphene nanosheets with superior shielding effect.[31] However, the feedstock for preparation of ionic liquid mentioned above was derived from chemical products with complex synthesis process.

L-Histidine, as a natural amino acid, is biodegradable and ecofriendly.[32] It contains a 1*H*-imidazole-4-ylmethyl group, which can be used as the maternal structure to fabricate ionic liquids. As far as we know, few reports have been found focus on the synthesis of L-histidine based ionic liquid (LHIL) and its application for corrosion inhibition. Herein, a novel LHIL was developed. The inhibitive performance of the LHIL on mild steel in 1 M HCl was evaluated by electrochemical measurements. The interaction and adsorption process of LHIL on steel surface were also proposed based on the experimental and

[a]*Institute of Oceanographic Instrumentation, Qilu University of Technology (Shandong Academy of Sciences), Shandong Provincial Key Laboratory of Marine Monitoring Instrument Equipment Technology, National Engineering and Technological Research Center of Marine Monitoring Equipment, 37 Miaoling Road, Qingdao 266061, China*

[b]*College of Materials Science and Engineering, Shandong University of Science and Technology, Qingdao 266590, China*

[c]*College of Chemistry and Pharmaceutical Sciences, Qingdao Agricultural University, Qingdao 266109, China. E-mail: bqian@qau.edu.cn*

† Electronic supplementary information (ESI) available. See DOI: 10.1039/d1ra08275b

© 2022 The Author(s). Published by the Royal Society of Chemistry

Open Access Article. Published on 21 January 2022. Downloaded on 1/21/2026 12:12:41 AM.
This article is licensed under a Creative Commons Attribution-NonCommercial 3.0 Unported Licence.

theoretical investigations. Our efforts might shed new light on the design of novel chemical structures as corrosion inhibitors.

2. Experimental

2.1 Materials

L-Histidine, di-*tert*-butyl dicarbonate, 1-bromohexane, and 1,4-dioxane were provided by Shanghai Aladdin Biochemical Technology Co., Ltd (Shanghai, China). Methanol and hydrochloric acid (38%) were obtained from Sinopharm Chemical Reagent Co., Ltd (Shanghai, China).

2.2 Synthesis of LHIL

The LHIL was synthesized through a two-step reaction, as shown in Fig. 1a. First, the amino-group in L-histidine molecular was protected by di-*tert*-butyl dicarbonate (step 1). Specifically, L-histidine was dissolved in deionized water with ultrasonic treatment. Then, the 1,4-dioxane solution containing equimolar di-*tert*-butyl dicarbonate was added drop by drop into the L-histidine aqueous solution under ice bath condition and stirred for 12 h. After removing the solvents, the product was purified by extraction with the mixture solution of ethyl acetate and deionized water. Then, the di-*tert*-butyl dicarbonate protected L-histidine (L-histidine-Boc) was obtained by removing the solvents.

For the synthesis of LHIL, the obtained L-histidine-Boc and 1-bromohexane were dissolved in methanol to receive a homogeneous solution. This reaction was carried out on an oil bath (363 K) with magnetic stirring for 24 h (step 2). The unreacted raw materials were removed by adding ethyl acetate. Finally, the LHIL was synthesized.

2.3 Electrode and solutions preparation

The testing substrate in this study was acted by Q235 mild steel. Before experiment, 400 and 800 SiC sand papers were employed to polish the steel to obtain a smooth surface. The corrosive

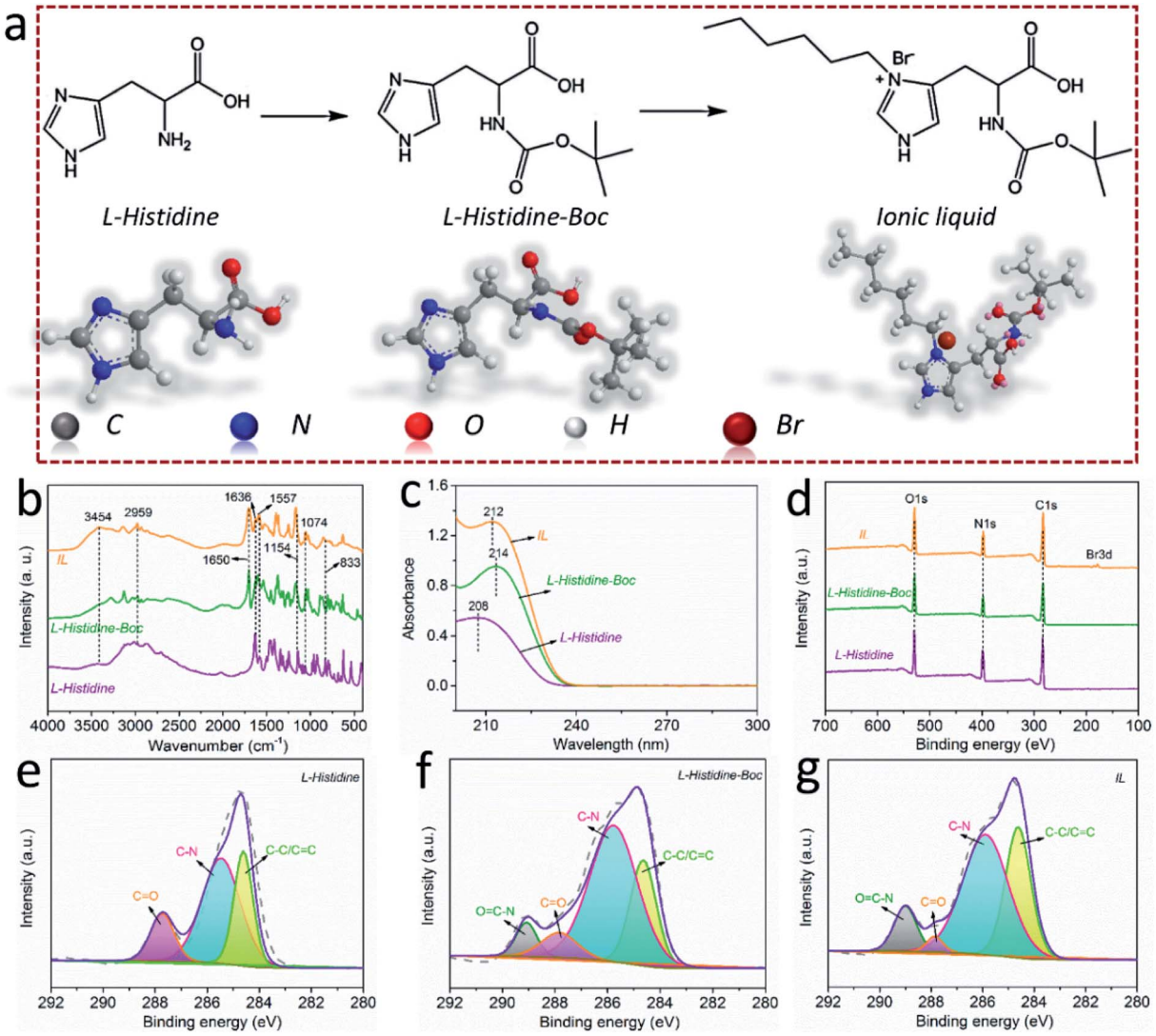

Fig. 1 (a) The synthesis route of LHIL. (b) FTIR, (c) UV-vis spectra and (d) XPS survey of L-histidine, L-histidine-Boc and LHIL; XPS high-resolution C 1s profiles of (e) L-histidine, (f) L-histidine-Boc and (g) LHIL.

 © 2022 The Author(s). Published by the Royal Society of Chemistry

Open Access Article. Published on 21 January 2022. Downloaded on 1/21/2026 12:12:41 AM.
This article is licensed under a Creative Commons Attribution-NonCommercial 3.0 Unported Licence.

medium was 1 M HCl without and containing different amount (0.5, 1, and 2 mM) of the LHIL. For comparison, the 1 M HCl solutions with different concentrations (0.5, 1, and 2 mM) of L-histidine were also prepared.

2.4 Characterization of LHIL

The molecular structure of the prepared LHIL was investigated by Fourier-transform infrared (Thermo Electron Scientific Instruments Corp., Nicolet 5700) spectroscopy. LHIL was also characterized by ^{1}H-NMR spectroscopy (JEOL Ltd, JNM-ECZ400S) in DMSO-d_6. The mass spectra of LHIL was evaluated by the high-resolution mass spectrometry (Thermo Fisher Scientific Inc., Thermo Scientific Q Exactive). Besides, UV absorption spectra were performed on Lambda 950 UV spectrophotometer. In addition, the chemical composition and bonding status were determined through X-ray photoelectron spectroscopy (XPS, AXIS ULTRA DLD).

2.5 Electrochemical investigations

A CHI660E electrochemical workstation was used to obtain the electrochemical measurements. The mild steel (1 × 1 cm^2), saturated calomel electrode (SCE), and a platinum plate (2 × 2 cm^2) were used as the working, reference, and counter electrode, respectively. The test temperature was controlled at 298 K and the test solutions were opened to the atmosphere. Before testing, the working electrode was placed in the studied solution for 1 h to achieve a stable Open Circuit Potential (OCP) value. EIS measurements were performed from 100 kHz to 100 mHz with a 5 mV sinusoidal perturbation. The EIS results were fitted with ZSimpWin software by plausible equivalent circuits. Tafel plots were recorded in the potential range from −250 mV to +250 mV *versus* OCP with a scan rate of 1 mV s^{-1}. In addition, the inhibition behavior of LHIL on localized corrosion of the mild steel was studied by scanning vibrating electrode technique (SVET). The current density values were collected on an area of 5 × 5 mm^2 with 26 × 26 scanning positions.

2.6 Surface analysis

Before and after immersion in the prepared corrosive solutions for 1 h, the surface morphologies and chemical compositions of the steels were observed by scanning electron microscopy (SEM, JEOL Ltd, 7001F) and energy dispersive spectroscopy (EDS). In addition, laser scanning confocal microscope (LSCM, LSM700) was used to examine the roughness of electrodes.

2.7 Calculation studies

L-Histidine and LHIL molecules were optimized at density functional theory (DFT) level to obtain the quantum chemical parameters by using DMol^3 module. In addition, the inhibition mechanism was also indicated by calculating the adsorption strength of inhibitor on steel, which was investigated by molecular dynamics (MD) method in Forcite module. In MD simulation, a simulation box consisting of five layers of Fe (110), one inhibitor molecule, 500 H_2O molecules, and 30 Å vacuum layer was established. The bonding energy between an inhibitor molecule and Fe (110) surface was calculated.

3. Results and discussion

3.1 Characterization of LHIL

The molecular structure of the synthesized LHIL was characterized by FTIR spectra, as shown in Fig. 1b. In case of L-histidine, the N–H stretching is at 3454 cm^{-1}. Besides, the evident absorption peaks locates at 1636, 1557 and 1074 cm^{-1} attribute to C=O anionic nature, imidazole ring vibrations of histidine and NH symmetrical stretching, respectively.[33] The typical peak of carboxylate anion (COO^-) stretching in the histidine molecular occurs at 1154 cm^{-1} and the NH_2 wagging vibration is at 833 cm^{-1}.[34] Compared with L-histidine, a prominent peak exhibits at 1650 cm^{-1} for L-histidine-Boc and LHIL, corresponding to amide bond (N–C=O).[35] Notably, the appearance of N–C=O proves that the amino group in L-histidine has been protected. It can be observed from the spectrum of LHIL the C–H bond deformation at 2959 cm^{-1} clearly enhanced.[36] This can be ascribed to the grated hexane chain, improving the C–H proportion in LHIL molecular structure and proving increased absorption intensity. UV-vis absorption spectra were also measured to analyze the synthesized LHIL. As observed in Fig. 1c, the characteristic absorption peak of L-histidine displays at about 208 nm, can be assigned to the π–π transition that originates from the C=C bond of the imidazole ring.[37,38] In terms of LHIL, the peak at 208 nm shifted to 212 nm, which may derive from the electronic conjugation in imidazole ring. The alkyl chain, as electron donating group, can alter the electron cloud density of conjugate structure after been chemically grafted on imidazole ring.

The bonds information (valence states and chemical compositions) of the samples during the synthesis process was analyzed by XPS measurements and the full XPS spectra of L-histidine, L-histidine-Boc and IL were presented in Fig. 1d. It can be found that their main element compositions are the same, C, O and N, while the proportion of these elements displays difference. Notably, the conspicuous peak of Br exhibits in the spectrum of LHIL compared with L-histidine, L-histidine-Boc, indicating the chemical grafting of 1-bromohexane. Accordingly, the high resolution of XPS spectra of C 1s of L-histidine, L-histidine-Boc and LHIL are presented in Fig. 1e–g. The C 1s spectrum of L-histidine presents three peaks at 284.6, 285.5 and 287.7 eV, relating to C–C/C=C, C–N and C=O bonds,[39] respectively. As can be seen, a new peak centered at 289 eV appears for L-histidine-Boc and LHIL, associating to O=C–N bond.[35] The presence of characteristic peak of O=C–N derives from the amide reaction between L-histidine and di-*tert*-butyl dicarbonate, which illustrates that the amine has been protected. After grafting 1-bromohexane, the content of C–C bond increases as compared with L-histidine-Boc, proving the successful synthesis of LHIL.

The successful prepared of LHIL was also confirmed by ^{1}H-NMR and high-resolution mass spectroscopy (HRMS) (Fig. S1 and S2†). In the ^{1}H-NMR, the characteristic H of amido bond appears at 7.7 ppm. The pentatomic ring of amino acid are in

Open Access Article. Published on 21 January 2022. Downloaded on 1/21/2026 12:12:41 AM.
This article is licensed under a Creative Commons Attribution-NonCommercial 3.0 Unported Licence.

the range of 6.5–7.0 ppm. The H in the Boc protecting group can be shown at 1.3 ppm. The methyl and methylene on the long chain are in the range of 1.0–1.5 ppm. HRMS spectrum of LHIL was given in Fig. S2.† The spectrum of LHIL is dominated by a M^+ ion at m/z 340.22. This peak is obtained by removing bromide ion.

3.2 Electrochemical studies

Polarization test was conducted to investigate the inhibition ability of synthesized LHIL for steel corrosion, presented in Fig. 2. Correspondingly, the related electrochemical elements are listed in Table 1, consisting of corrosion potential (E_{corr}), corrosion current density (i_{corr}), anodic Tafel slope (β_a) and cathodic Tafel slope (β_c). Besides, the inhibition efficiency (η) and the surface coverage (θ) are deduced according to the equations:

$$\eta\ (\%) = \frac{i^0_{corr} - i'_{corr}}{i^0_{corr}} \times 100 \quad (1)$$

$$\theta = \frac{i^0_{corr} - i'_{corr}}{i^0_{corr}} \quad (2)$$

where i^0_{corr} and i'_{corr} represent the corrosion current densities of Q235 steel in the absence and presence of the inhibitors,[40,41] respectively.

In Fig. 2a, the addition of L-histidine results little decrease in the current density value, which reveals that the L-histidine molecular has little corrosion inhibition function on steel in this condition. However, with the introduction of LHIL, as exhibited in Fig. 2b, the cathodic current density is significantly reduced. In addition, the cathodic branches of the polarization plots change to low current density range as the LHIL content increases, while little change is observed in the anodic branches. It is noted that the corrosion current density decreases from 2070 μA cm^{-2} (blank solution) to 22.91 μA cm^{-2} within the LHIL containing solution (2 mM), demonstrating their efficient corrosion inhibition function. Moreover, a negative trend in corrosion potential presents along with the addition of LHIL. In Table 1, the steel in HCl solution with 2 mM LHIL presents the lowest corrosion potential value (−445 mV) among samples, which indicates that the synthesized LHIL can be defined as a moderate cathodic-type corrosion inhibitor. These observations clearly demonstrate that the LHIL molecular can serve as a high efficient inhibitor by suppressing the cathodic oxygen reduction process.[42,43]

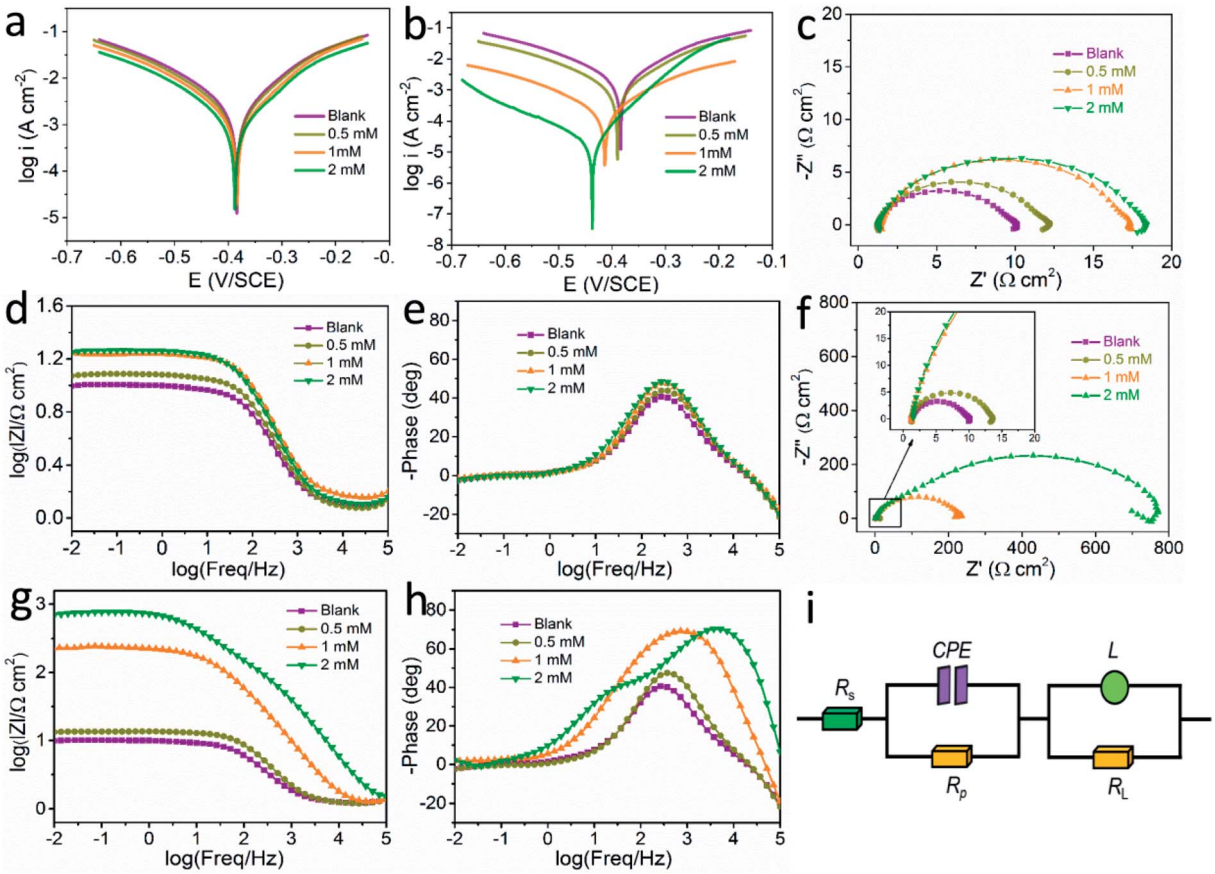

Fig. 2 Potentiodynamic polarization curves for Q235 steel in 1 M HCl solution without and with different concentrations of (a) L-histidine and (b) LHIL. Nyquist and Bode plots for the steel samples immersed in 1 M HCl solution containing different concentration of (c–e) L-histidine and (f–h) LHIL. (i) Equivalent circuit used to fit the EIS data.

 © 2022 The Author(s). Published by the Royal Society of Chemistry

Open Access Article. Published on 21 January 2022. Downloaded on 1/21/2026 12:12:41 AM.
This article is licensed under a Creative Commons Attribution-NonCommercial 3.0 Unported Licence.

Table 1 Potentiodynamic polarization parameters of mild steel in 1 M HCl solution without and with different concentrations of L-histidine and LHIL

C (mM)	E_{corr} (mV)	i_{corr} (μA cm^{-2})	β_a (mV dec^{-1})	β_c (mV dec^{-1})	η	θ
Blank	−382	2070	108	−138	—	—
L-Histidine						
0.5	−379	1550	103	−135	25.0	0.25
1	−377	1310	97	−132	36.5	0.365
2	−385	1010	95	−133	51.1	0.511
LHIL						
0.5	−386	977.2	104	−136	52.8	0.528
1	−421	426.4	116	−135	79.4	0.794
2	−445	22.91	64	−143	98.8	0.988

Generally, polarization curves can be separate into two branches: anodic and cathodic. The anodic branch is relates to the metal dissolution, whereas the cathodic branch corresponds to the reduction process of oxidizing species (oxygen and hydrogen ion).[44] As shown in Table 1, the cathodic slopes remain basically steady with the addition of LHIL, which illustrates that the mechanism of cathodic reaction is not influenced by introducing LHIL. On the contrary, an obvious impact on the anodic slop value presents when the concentration of LHIL reached 2 mM. Therefore, the inhibition behavior of LHIL on steel is mainly rely on lowering the current density. These findings prove that a relative stable LHIL-adsorption layer on steel can be formed, thus exhibiting a barrier against aggressive mediums to provide efficient inhibitive capability for steel in HCl condition.[45]

To investigate the surface process of the electrode, EIS test was performed on steel after 1 h immersion and the results were presented in Fig. 2c–h. It is clear that all the collected plots show the similar appearance whether there is inhibitors. This reveals that the electrochemical behavior of the tested solution does not been changed, which may ascribed to the relative loose property of the adsorbed LHIL film. As can be seen from the Nyquist plots in Fig. 2c and f, a decreased capacitive semicircle at high frequency (HF) accompanied with a small inductive loop in low frequency (LF) present. Usually, the HF capacitive loop is owing to the double layer properties, and the LF inductive loop is associated with the relaxation process of aggressive ions at the steel surface.[4,46] The addition of L-histidine into HCl solution slightly increases the capacitive loop, indicating the limited corrosion inhibitive function of pure L-histidine for mild steel in this conditions. Interestingly, an obvious enlarge in the diameter of high-frequency loop exhibits with introducing synthesized LHIL inhibitors (Fig. 2f). This phenomenon becomes more apparent when the concentration of LHIL is increased to 2 mM. These results demonstrate that the LHIL molecular can form protective layer on the steel surface to inhibit the charge transfer process.

The protective performance of LHIL on steel can also be reflected from the Bode plots, as shown in Fig. 2g. In general, the impedance value at low frequency can be considered as an index to weigh the protective performance of inhibitors. The impedance values at low frequency improve with increase of LHIL content. When the LHIL concentration is 2 mM, their impedance value is greatly increased. In addition, the expansion of LHIL content induces a larger frequency range with the maximum phase angle. These observations proves that the LHIL effectively inhibited the corrosion reaction of steel.

The electrochemical results was also analyzed using the corresponding equivalent circuit in Fig. 2i. As for equivalent circuit, R_s is the solution resistance. R_p (polarization resistance) is used to stand for all kinds of resistances between the metal and solution. L and R_L correspond to the inductance and related resistance. Due to the non-ideal frequency responsive property, constant phase element (CPE) is selected to indicate the frequency dispersion characteristic instead of pure capacitor.[47,48] Accordingly, the impedance vale of CPE is determined below:

$$Z_{CPE} = Y_0^{-1}(jw)^{-n} \tag{3}$$

where Y_0 stands for the modulus of CPE, while the exponent n is to indicate the deviation degree. The can represent resistor, capacitor and inductor when the value of n is equal to 0, 1 and −1, respectively. Besides, j is the imaginary part and w is the angular frequency.[49]

Table 2 Impedance parameters and inhibition efficiency of mild steel in 1 M HCl in the absence and presence of studied inhibitors after 1 h immersion

C (mM)	R_s (Ω cm^2)	CPE (μF cm^{-2})	n	R_p (Ω cm^2)	η
Blank	1.20	664	0.82	8.77	—
L-Histidine					
0.5	1.16	523	0.83	10.88	19.4
1	1.43	432	0.85	12.88	31.9
2	1.24	328	0.83	17.01	48.4
LHIL					
0.5	1.21	310	0.87	12.28	28.6
1	1.06	73.6	0.83	233	96.2
2	1.34	58.3	0.81	755	98.8

Open Access Article. Published on 21 January 2022. Downloaded on 1/21/2026 12:12:41 AM.
This article is licensed under a Creative Commons Attribution-NonCommercial 3.0 Unported Licence.

Table 3 Comparison of the inhibition efficiency of LHIL with the literature data as corrosion inhibitors for mild steel in 1 M HCl

Inhibitor	Concentration	Efficiency at room temperature (%)	References
Iminium surfactant	0.5 mM	90.6	52
Isoxazolidine derivatives	100 mg L^{-1}	80.5	53
4-(Pyridin-4-yl)thiazol-2-amine	0.2 mM	96.6	54
Aniline trimer-including β-cyclodextrin	200 mg L^{-1}	98.5	55
Vanillin Schiff bases	1 mM	94.0	56
Chromeno-carbonitriles	1 mM	95.3	57
Sugarcane purple rind extract	800 mg L^{-1}	94.1	58
Castor oil-based inhibitor	140 μM	82.0	59
LHIL	2 mM	98.8	Present study

The fitted results were summarized in Table 2. Thus, the corrosion inhibition efficiency (η) of LHIL for steel can be obtained from charge transfer parameters based on the following equation:

$$\eta\ (\%) = \frac{R'_p - R^0_p}{R'_p} \times 100 \quad (4)$$

where R^0_p and R'_p indicate the polarization resistance without and with inhibitors, respectively. Obviously, the introduction of LHIL results in the decrease in CPE values. The decrease of CPE can be attributed to the adsorption of LHIL molecular, which could cover the electrode surface and increase the electric double-layer thickness.[50,51] On the other hand, the presence of LHIL increases the R_p values and especially prominent in LHIL 2 mM (increased by nearly two order of magnitude compared with blank sample). It can be speculated that LHIL molecules interact with steel electrode to form protective layers and thus the water molecules and other adsorbed ions were displaced by the LHIL films. These observations indicate that the LHIL could provide effective corrosion inhibition function for steel by formation adsorption layer to retard the electrochemical transfer process. The compare of LHIL with earlier studied inhibitors[52–59] on the inhibition efficiency was shown in Table 3. LHIL exhibites better corrosion inhibition behaviors.

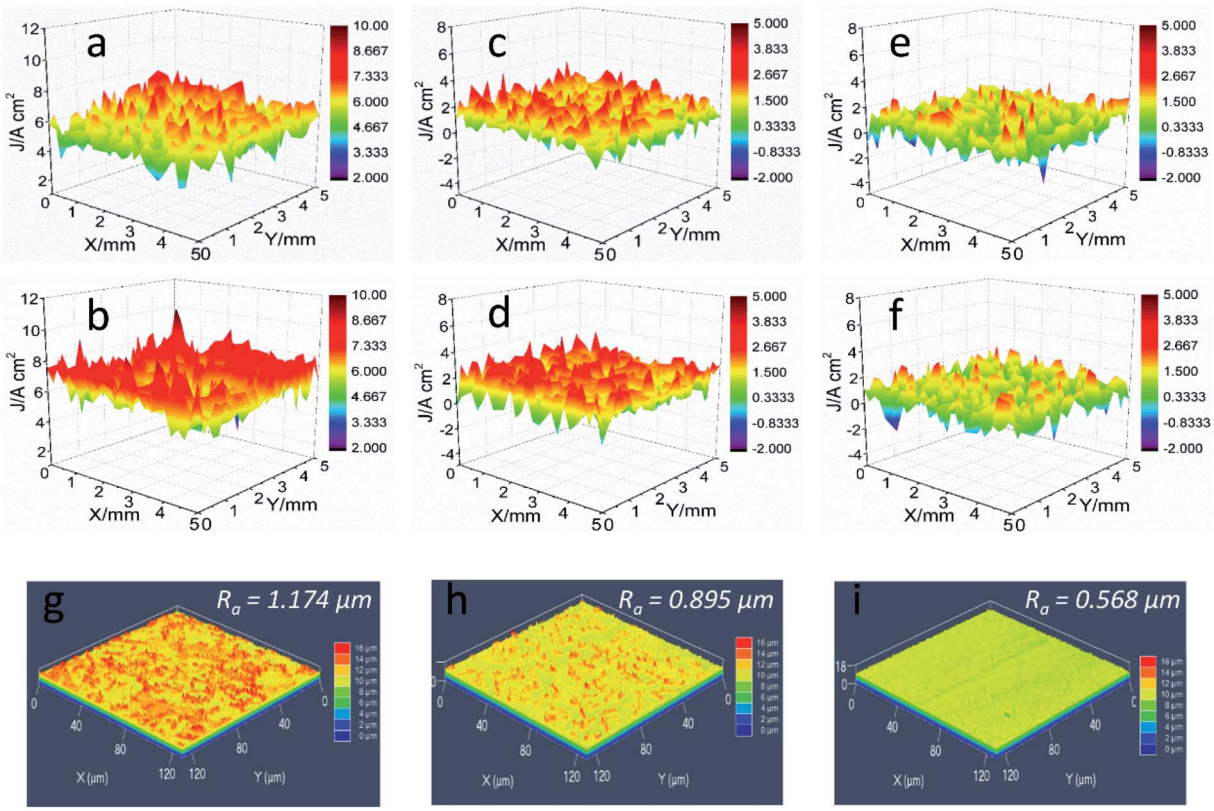

Fig. 3 SVET results of steel in different solutions: (a) blank-1 h, (b) blank-3 h, (c) L-histidine-1 h, (d) L-histidine-3 h, (e) LHIL-1 h, (f) LHIL-3 h. The surface roughness (R_a) of steel electrodes after 3 h immersion in 1 M HCl solution without (g) and with 2 mM of L-histidine (h) and 2 mM of LHIL (i).

 © 2022 The Author(s). Published by the Royal Society of Chemistry

Open Access Article. Published on 21 January 2022. Downloaded on 1/21/2026 12:12:41 AM.
This article is licensed under a Creative Commons Attribution-NonCommercial 3.0 Unported Licence.

3.3 Localized corrosion analysis and surface investigations

The integrity of formed films on the steel plays a key role in their corrosion inhibition activity. SVET test was carried out to determine the localized corrosion of mild steel by mapping the current density within a defined area, as shown in Fig. 3. The potential signals among the selected area were obtained and then transferred into the local current density. For blank HCl solution, positive current density presents at the tested range (Fig. 3a), which can be ascribed to severe anodic corrosion. After 3 h immersion, higher current density detected with uneven distribution property, exhibiting the typical localized corrosion. The addition of L-histidine causes the reduction of anodic current density to a certain extent, whereas their current values also maintained at a high reactivity degree (Fig. 3d). On the contrary, a distinct decrease in the anodic current density is observed for the steel electrode in LHIL containing HCl solution (Fig. 3e). Even after 3 h immersion, no obvious variation in anodic corrosion reaction detected, revealing the suppression of electrochemical reaction. These findings prove the superior corrosion inhibitive function of LHIL for mild steel from in-suit and localized electrochemical process, and prove the strong adsorption capability of LHIL on steel surface.

The surface roughness (R_a) of samples after SVET test was determined through LSCM to reveal the corrosion inhibition ability the LHIL. As can be seen in Fig. 3g, the polished steel presents a high R_a value (1.174 μm) after 3 h immersion, indicating the sever corrosion. In terms of the HCl solution containing L-histidine, some decrease in the R_a (0.895 μm) value is appeared, compared with pure HCl solution. On the contrary, a relative neat surface with small R_a value (0.568 μm) is observed. These results demonstrate that the synthesized LHIL can effectively protect steel in HCl by forming protective layers on the steel.

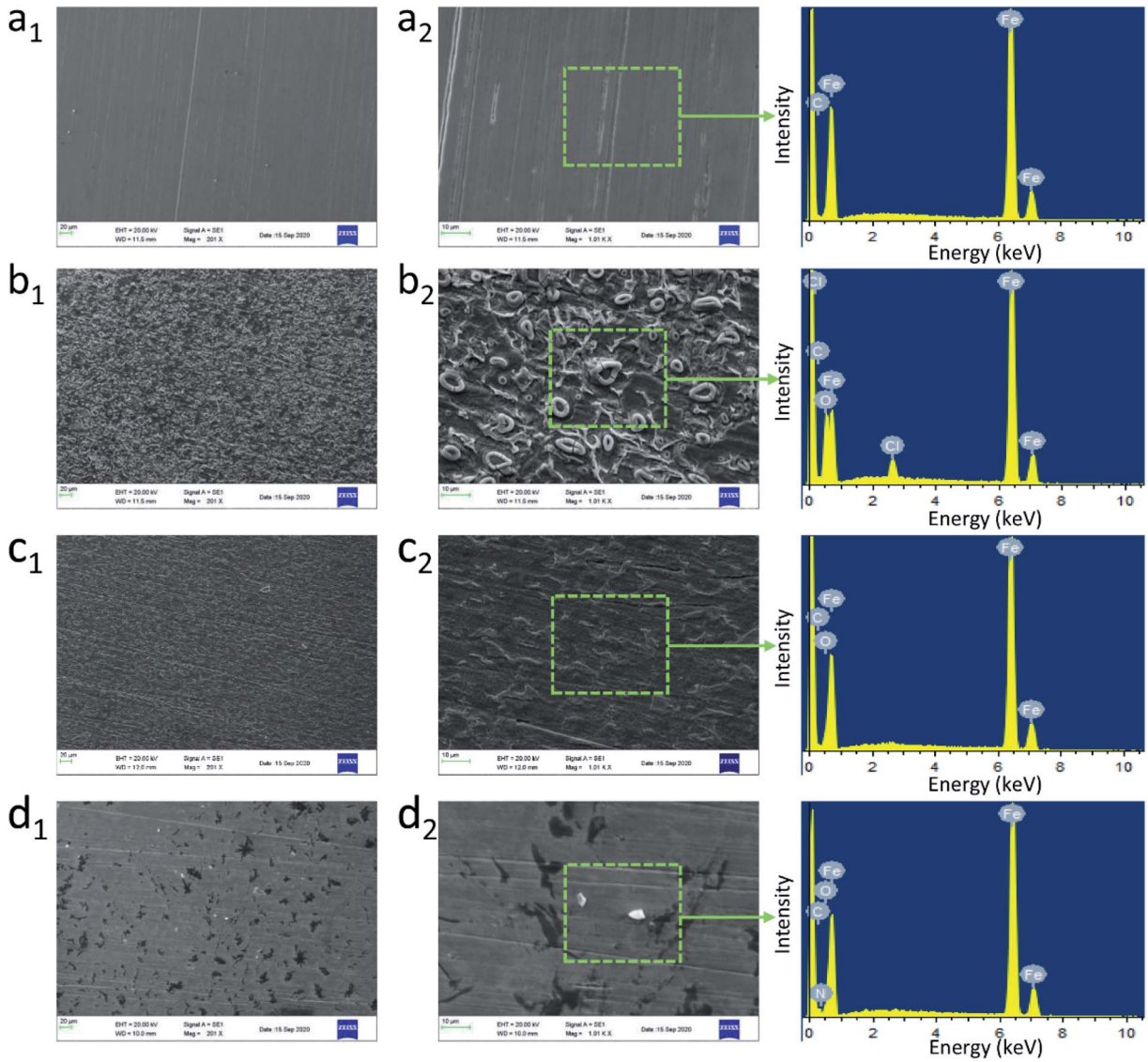

Fig. 4 Morphology and corresponding EDS spectra of the polished mild steel (a) and steel electrodes after 1 h immersion in 1 M HCl solution without (b) and with 2 mM of L-histidine (c) and 2 mM of LHIL (d).

Open Access Article. Published on 21 January 2022. Downloaded on 1/21/2026 12:12:41 AM.
This article is licensed under a Creative Commons Attribution-NonCommercial 3.0 Unported Licence.

In addition, the surface morphology of steel in pure HCl and LHIL containing solutions was explored by SEM examination, as observed in Fig. 4. From Fig. 4a, the steel surface is smooth with clear scratches derived from polishing process. As is shown in Fig. 4b, the unprotected steel specimen is covered by many corrosion products with clear pits after immersed for 1 h, which indicates that the Q235 steel is seriously corroded. Although the amount of corrosion byproducts on the steel decreases with the addition of L-histidine, the cluster, pits and cracks are also formed (Fig. 4c). This illustrates the limited corrosion inhibitive function of L-histidine. In the presence of LHIL, on the contrary, the steel surface is effectively protected without obvious corrosion products (Fig. 4d). In addition, the steel surface is smoother than other samples. Therefore, it can be concluded that the corrosion attack is effectively suppressed by LHIL adsorbed layers.

To examine the inhibitive film on the mild steel, the surface composition of the electrodes after 1 h immersion under different conditions was obtained by EDS spectra. In addition, the corresponding surface composition was collected as displayed in Fig. S3.† The main components of the studied steel is C (8.29 wt%) and Fe (91.71 wt%). For electrode immersed in 1 M HCl (Fig. S3†), the intensity of Fe element decreases to 75.23 wt%, which indicates the oxidation and dissolution of Fe. The characteristic peaks for Cl and O appear at the spectrum of steel for blank solution. The high content of Cl and O elements reveals the steel is seriously corroded by the aggressive solution. As for the sample immersed in LHIL containing solution (Fig. S3†), the EDS spectrum and elemental composition are different. The appearance of N element, derived from the adsorbed LHIL molecules, provides the evidence for the formation of inhibitive films. In addition, an increase in the C content (11.07 wt%) is also detected, which can be ascribed to the formation of LHIL film on steel surface. The synthesized LHIL inhibitor with imidazole ring and alkyl chain, which obviously changes the surface composition of steel surface.

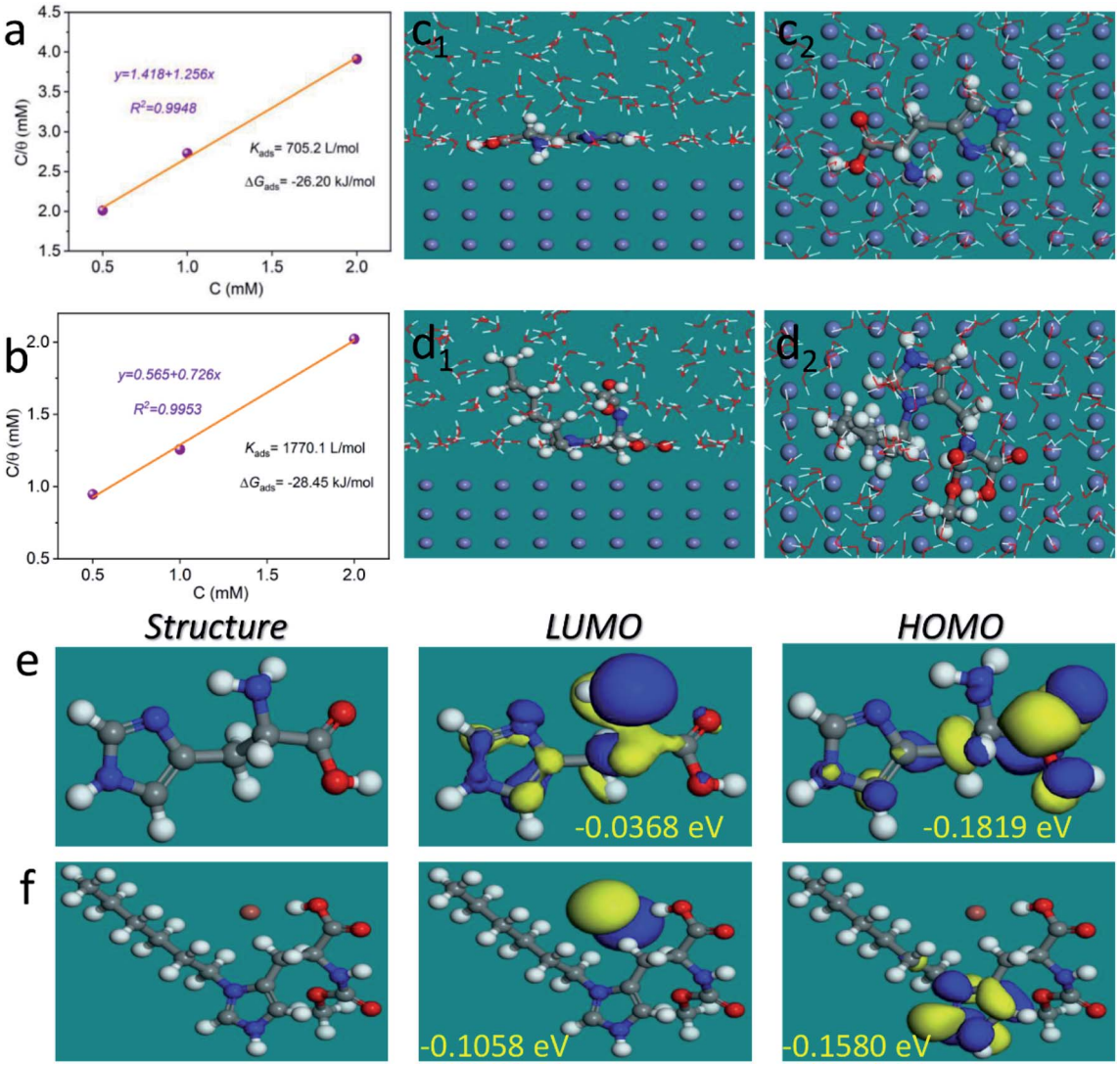

Fig. 5 Langmuir adsorption isotherms and the corresponding thermodynamic parameters of L-histidine (a) and LHIL (b) on the mild steel surface in 1 M HCl solution. Equilibrium adsorption configurations of inhibitor molecule on Fe (110) surface (c) L-histidine and (d) LHIL. The optimized structures and frontier orbital density distributions for (e) L-histidine and (f) LHIL.

 © 2022 The Author(s). Published by the Royal Society of Chemistry

Open Access Article. Published on 21 January 2022. Downloaded on 1/21/2026 12:12:41 AM. This article is licensed under a Creative Commons Attribution-NonCommercial 3.0 Unported Licence.

From these findings, it can be speculated that the LHIL serves as high performance corrosion inhibitor to prevent the steel from HCl attack by formation protective film, leading to the decrease in the steel degradation.

3.4 Adsorption isotherm and theoretical studies

To further analyze the protective mechanism of the LHIL for mild steel, the adsorption isotherms were calculated through matching the surface coverage to LHIL concentration. It is found that the results of potentiodynamic polarization measurements are well accord to Langmuir isotherm with linear regression coefficients (R^2) close to 1, which deducts based on the eqn (5):

$$\frac{\theta}{1-\theta} = K_{\text{ads}} C \tag{5}$$

where θ is the degree of the coverage, C is the concentration of inhibitor. K_{ads} represents the equilibrium constant of the adsorption process.[60]

Fig. 5a and b displays a straight line plotted by C *versus* C/θ. The K_{ads} value can be achieved from the reciprocal of intercept. The standard adsorption free energy ΔG_{ads} can be calculated as follows:

$$K_{\text{ads}} = \frac{1}{55.5} \exp \frac{-\Delta G^0_{\text{ads}}}{RT} \tag{6}$$

R is the molar gas constant and T is the tested temperature.[61] The calculated K_{ads} and ΔG^0_{ads} are presented. It is considered that the high K_{ads} value and low ΔG^0_{ads} value imply a better adsorption ability of compounds on steel. The modes of adsorption of inhibitors can be differentiated based on the ΔG^0_{ads} values. When the ΔG^0_{ads} value is more than -20 kJ mol^{-1}, the adsorption can be defined as physisorption resulted from electrostatic interaction. The ΔG^0_{ads} value of chemisorption is around -40 kJ mol^{-1} or more negative, which corresponds to the electronic bond between the surface and the adsorbate.[62] In our study, the ΔG^0_{ads} values of L-histidine and LHIL are ranging from -26 to -29 kJ mol^{-1}, which indicates that LHIL adsorb by both chemisorption and physisorption.

To further illustrate the interfacial interaction of inhibitors on metal surface and reveal the inhibition mechanism, MD simulations were performed to provide the equilibrium adsorption configurations on Fe (110) surface. As is shown in Fig. 5c and d, both L-histidine and LHIL are tightly adsorbed on the steel surface with a parallel orientation. As a result, a coordination bond could form, which is derived from the electrons transfer from imidazole ring to the empty orbit of steel surface.[63] Simultaneously, the parallel arranged inhibitors can cover the steel surface as much as possible, reducing the contact area of steel with electrolytes. Moreover, the adsorption strength of inhibitor on metal can be determined from the binding energy (E_{binding}). Form the calculation, the E_{binding} of LHIL is 303.47 kcal mol^{-1}, while the E_{binding} of L-histidine is 115.71 kcal mol^{-1}. The higher E_{binding} value implies a superior inhibition efficiency. These results confirm the strong inhibition ability of prepared LHIL, providing theoretical evidence for above results.

The influence of electronic structure of molecules on their inhibitive performance was analyzed through quantum chemical study. Fig. 5e and f present the optimized structures, the highest occupied molecular orbital (HOMO) and the lowest unoccupied molecular orbital (LUMO) for L-histidine and LHIL, respectively. Generally, the HOMOs of LHIL spread mainly on the alkyl chain. It is considered that the E_{HOMO} presents the electron donating ability, whereas the E_{LOMO} value reveals the electron absorption ability.[64] Besides, the reactivity of molecule can be reflected from the energy gap ($\Delta E = E_{\text{HOMO}} - E_{\text{LOMO}}$).[65] Usually, a lower value denotes a higher inhibition effect. As expected, the as-prepared LHIL exhibits lower ΔE value (0.0522 eV) than that of L-histidine (0.1451 eV), demonstrating its higher inhibitive property. These results are in good agreement with the electrochemical results.

4. Conclusion

In summary, a novel LHIL has been successfully synthesized, which acts as a high efficient sustainable corrosion inhibitor for steel in acid. Comprehensive investigations were performed to evaluate the inhibitive capability and protection mechanism of LHIL for mild steel. Electrochemical results indicates that the LHIL serves as a modest cathodic-type inhibitor and provides effective inhibition function for steel in 1 M HCl solution. The η obtained from Tafel curves improves with the increase of LHIL content, and the η value reaches to 98.8% for 2 mM LHIL after 1 h. The adsorption of studied LHIL on steel surface obeys the Langmuir adsorption isotherm, consisting of chemisorption and physisorption. The imidazole cations interact with the pre-adsorbed anions (Br^- and Cl^-) to arrive the steel surface and then result in the chemical interaction with substrate, which contributing to the formation of compact protective film. Surface evaluation combined with EDS and Raman spectra analysis persuasively support the speculated mechanism, which proves that the superior protection performance of LHIL is achieved by forming a dense and barrier film. Theoretical results indicate that the prepared LHIL possesses low ΔE and high E_{binding}, revealing its strong absorption and superior inhibition properties.

Conflicts of interest

There are no conflicts to declare.

Acknowledgements

This work was funded by National Natural Science Foundation of China (51801110).

References

1 W. Guo, A. Umar, Q. Zhao, M. A. Alsaiari, Y. Al-Hadeethi, L. Wang and M. Pei, Corrosion inhibition of carbon steel by three kinds of expired cephalosporins in 0.1 M H_2SO_4, *J. Mol. Liq.*, 2020, **320**, 114295.

Open Access Article. Published on 21 January 2022. Downloaded on 1/21/2026 12:12:41 AM.
This article is licensed under a Creative Commons Attribution-NonCommercial 3.0 Unported Licence.

2 D. Daoud, T. Douadi, H. Hamani, S. Chafaa and M. Al-Noaimi, Corrosion inhibition of mild steel by two new S-heterocyclic compounds in 1 M HCl: experimental and computational study, *Corros. Sci.*, 2015, **94**, 21–37.
3 I. B. Obot, A. Meroufel, I. B. Onyeachu, A. Alenazi and A. A. Sorour, Corrosion inhibitors for acid cleaning of desalination heat exchangers: progress, challenges and future perspectives, *J. Mol. Liq.*, 2019, **296**, 111760.
4 A. Khadiri, A. Ousslim, K. Bekkouche, A. Aouniti and B. Hammouti, Inhibition Effects on the Corrosion of Mild Steel in 1 M HCl by 1,1'-(2,2'-(2,2'-oxybis(ethane-2,1-diyl) bis(sulfanediyl)) bis(ethane-2,1-diyl))diazepan-2-one, *Port. Electrochim. Acta*, 2014, **32**, 35–50.
5 M. Goyal, S. Kumar, I. Bahadur, C. Verma and E. E. Ebenso, Organic corrosion inhibitors for industrial cleaning of ferrous and non-ferrous metals in acidic solutions: a review, *J. Mol. Liq.*, 2018, **256**, 565–573.
6 Y. Gong, L. Zhang, C. Jing, F. Gao, S. Zhang and H. Li, Self-assembly of new dendrimers basing on strong π-π intermolecular interaction for application to protect copper, *Chem. Eng. J.*, 2018, **342**, 238–250.
7 M. Cui, S. Ren, Q. Xue, H. Zhao and L. Wang, Carbon dots as new eco-friendly and effective corrosion inhibitor, *J. Alloys Compd.*, 2017, **726**, 680–692.
8 Y. Qiang, H. Li and X. Lan, Self-assembling anchored film basing on two tetrazole derivatives for application to protect copper in sulfuric acid environment, *J. Mater. Sci. Technol.*, 2020, **52**, 63–71.
9 Y. Qiang, S. Zhang, H. Zhao, B. Tan and L. Wang, Enhanced anticorrosion performance of copper by novel N-doped carbon dots, *Corros. Sci.*, 2019, **161**, 108193.
10 Y. Ye, D. Zhang, Y. Zou, H. Zhao and H. Chen, A feasible method to improve the protection ability of metal by functionalized carbon dots as environment-friendly corrosion inhibitor, *J. Cleaner Prod.*, 2020, **264**, 121682.
11 K. F. Khaled and N. Hackerman, Ortho-substituted anilines to inhibit copper corrosion in aerated 0.5 M hydrochloric acid, *Electrochim. Acta*, 2004, **49**, 485–495.
12 Y. Qiang, S. Zhang, B. Tan and S. Chen, Evaluation of Ginkgo leaf extract as an eco-friendly corrosion inhibitor of X70 steel in HCl solution, *Corros. Sci.*, 2018, **133**, 6–16.
13 G. Sigircik, T. Tuken and M. Erbil, Inhibition efficiency of aminobenzonitrile compounds on steel surface, *Appl. Surf. Sci.*, 2015, **324**, 232–239.
14 S. Ghaderi, S. A. Haddadi, S. Davoodi and M. Arjmand, Application of sustainable saffron purple petals as an eco-friendly green additive for drilling fluids: a rheological, filtration, morphological, and corrosion inhibition study, *J. Mol. Liq.*, 2020, **315**, 113707.
15 M. T. Zaky, M. I. Nessim and M. A. Deyab, Synthesis of new ionic liquids based on dicationic imidazolium and their anti-corrosion performances, *J. Mol. Liq.*, 2019, **290**, 111230.
16 B. Qian, J. Wang, M. Zheng and B. Hou, Synergistic effect of polyaspartic acid and iodide ion on corrosion inhibition of mild steel in H_2SO_4, *Corros. Sci.*, 2013, **75**, 184–192.
17 Y. Tang, F. Zhang, S. Hu, Z. Cao, Z. Wu and W. Jing, Novel benzimidazole derivatives as corrosion inhibitors of mild steel in the acidic media. Part I: gravimetric, electrochemical, SEM and XPS studies, *Corros. Sci.*, 2013, **74**, 271–282.
18 Z. Liu, Y. Ye and H. Chen, Corrosion inhibition behavior and mechanism of N-doped carbon dots for metal in acid environment, *J. Cleaner Prod.*, 2020, **270**, 122458.
19 A. Y. El-Etre, M. Abdallah and Z. E. El-Tantawy, Corrosion inhibition of some metals using lawsonia extract, *Corros. Sci.*, 2005, **47**, 385–395.
20 A. Popova, M. Christov and A. Vasilev, Inhibitive properties of quaternary ammonium bromides of N-containing heterocycles on acid mild steel corrosion. Part I: gravimetric and voltammetric results, *Corros. Sci.*, 2007, **49**, 3276–3289.
21 N. V. Likhanova, P. Arellanes-Lozada, O. Olivares-Xometl, H. Hernández-Cocoletzi, I. V. Lijanova, J. Arriola-Morales and J. E. Castellanos-Aguila, Effect of organic anions on ionic liquids as corrosion inhibitors of steel in sulfuric acid solution, *J. Mol. Liq.*, 2019, **279**, 267–278.
22 C. Verma, I. B. Obot, I. Bahadur, E.-S. M. Sherif and E. E. Ebenso, Choline based ionic liquids as sustainable corrosion inhibitors on mild steel surface in acidic medium: gravimetric, electrochemical, surface morphology, DFT and Monte Carlo simulation studies, *Appl. Surf. Sci.*, 2018, **457**, 134–149.
23 E. A. Noor, Evaluation of inhibitive action of some quaternary N-heterocyclic compounds on the corrosion of Al-Cu alloy in hydrochloric acid, *Mater. Chem. Phys.*, 2009, **114**, 533–541.
24 M. Lashkari and M. R. Arshadi, DFT studies of pyridine corrosion inhibitors in electrical double layer: solvent, substrate, and electric field effects, *Chem. Phys.*, 2004, **299**, 131–137.
25 M. E. Palomar, C. O. Olivares-Xometl, N. V. Likhanova and J.-B. Pérez-Navarrete, Imidazolium, Pyridinium and Dimethyl-Ethylbenzyl Ammonium Derived Compounds as Mixed Corrosion Inhibitors in Acidic Medium, *J. Surfactants Deterg.*, 2011, **14**, 211–220.
26 A. A. Nkuna, E. D. Akpan, I. B. Obot, C. Verma, E. E. Ebenso and L. C. Murulan, Impact of selected ionic liquids on corrosion protection of mild steel in acidic medium: experimental and computational studies, *J. Mol. Liq.*, 2020, **314**, 113609.
27 Y. Qiang, S. Zhang, L. Guo, X. Zheng, B. Xiang and S. Chen, Experimental and theoretical studies of four allyl imidazolium-based ionic liquids as green inhibitors for copper corrosion in sulfuric acid, *Corros. Sci.*, 2017, **119**, 68–78.
28 X. Zheng, S. Zhang, W. Li, M. Gong and L. Yin, Experimental and theoretical studies of two imidazolium-based ionic liquids as inhibitors for mild steel in sulfuric acid solution, *Corros. Sci.*, 2015, **95**, 168–179.
29 T. L. Greaves and C. J. Drummond, Protic Ionic Liquids: Evolving Structure-Property Relationships and Expanding Applications, *Chem. Rev.*, 2015, **115**, 11379–11448.
30 C. Verma, E. E. Ebenso and M. A. Quraishi, Ionic liquids as green and sustainable corrosion inhibitors for metals and alloys: an overview, *J. Mol. Liq.*, 2017, **233**, 403–414.

 © 2022 The Author(s). Published by the Royal Society of Chemistry

Open Access Article. Published on 21 January 2022. Downloaded on 1/21/2026 12:12:41 AM.
This article is licensed under a Creative Commons Attribution-NonCommercial 3.0 Unported Licence.

31 C. Liu, S. Qiu, P. Du, H. Zhao and L. Wang, Ionic liquid-graphene oxide hybrid nanomaterial: synthesis and anticorrosive applications, *Nanoscale*, 2018, **10**, 8115–8124.
32 M. Bobina, A. Kellenberger, J. P. Millet, C. Muntean and N. Vaszilcsin, Corrosion resistance of carbon steel in weak acid solutions in the presence of L-histidine as corrosion inhibitor, *Corros. Sci.*, 2013, **69**, 389–395.
33 F. D. S. Franco, D. S. Fernandes and D. R. D. Carmo, A modified hybrid silsesquioxane/histidine composite for copper and zinc adsorption and it behavior in the electro-oxidation of ascorbic acid, *Mater. Sci. Eng., C*, 2020, **111**, 110739.
34 J. G. Mesu, T. Visser, F. Soulimani and B. M. Weckhuysen, Infrared and Raman spectroscopic study of pH-induced structural changes of L-histidine in aqueous environment, *Vib. Spectrosc.*, 2005, **39**, 114–125.
35 R. S. Zambare, X. Song, B. N. Sowrirajalu, A. P. James Selvaraj and P. R. Nemade, Ultrafast Dye Removal Using Ionic Liquid-Graphene Oxide Sponge, *ACS Sustainable Chem. Eng.*, 2017, **5**, 6026–6035.
36 K. Rajarajan, K. Anbarasan, J. S. Solomon and G. Madhurambal, XRD and FT-IR Studies on Lead (II) Nitrate doped Histidine Picrate crystal: A nonlinear optical material, *J. Chem. Pharm. Res.*, 2012, **4**, 4060–4065.
37 R. Katoh, Absorption Spectra of Imidazolium Ionic Liquids, *Chem. Lett.*, 2007, **36**, 1256–1257.
38 I. Tanabe, Y. Kurawaki, Y. Morisawa and Y. Ozaki, Electronic absorption spectra of imidazolium-based ionic liquids studied by far-ultraviolet spectroscopy and quantum chemical calculations, *Phys. Chem. Chem. Phys.*, 2016, **18**, 22526–22530.
39 Z. Wang, R. Young, J. R. Deng, L. Yang and F. Hao, Control of the functionality of graphene oxide for its application in epoxy nanocomposites, *Polymer*, 2013, **54**, 6437–6446.
40 M. A. Amin, K. F. Khaled and S. A. Fadl-Allah, Testing validity of the Tafel extrapolation method for monitoring corrosion of cold rolled steel in HCl solutions – experimental and theoretical studies, *Corros. Sci.*, 2010, **52**, 140–151.
41 E. Kowsari, S. Y. Arman, M. H. Shahini, H. Zandi, A. Ehsani, R. Naderi, A. Pourghasemihanza and M. Mehdipour, In situ synthesis, electrochemical and quantum chemical analysis of an amino acid-derived ionic liquid inhibitor for corrosion protection of mild steel in 1M HCl solution, *Corros. Sci.*, 2016, **112**, 73–85.
42 A. Yurt and O. Aykin, Diphenolic Schiff bases as corrosion inhibitors for aluminium in 0.1 M HCl: potentiodynamic polarisation and EQCM investigations, *Corros. Sci.*, 2011, **53**, 3725–3732.
43 B. Qian, B. Hou and M. Zheng, The inhibition effect of tannic acid on mild steel corrosion in seawater wet/dry cyclic conditions, *Corros. Sci.*, 2013, **72**, 1–9.
44 M. A. Amin, S. S. A. El-Rehim, E. E. F. El-Sherbini, O. A. Hazzazi and M. N. Abbas, Polyacrylic acid as a corrosion inhibitor for aluminium in weakly alkaline solutions. Part I: weight loss, polarization, impedance EFM and EDX studies, *Corros. Sci.*, 2009, **51**, 658–667.
45 Y. Qiang, S. Zhang, S. Yan, X. Zou and S. Chen, Three indazole derivatives as corrosion inhibitors of copper in a neutral chloride solution, *Corros. Sci.*, 2017, **126**, 295–304.
46 L. Hu, S. Zhang, W. Li and B. Hou, Electrochemical and thermodynamic investigation of diniconazole and triadimefon as corrosion inhibitors for copper in synthetic seawater, *Corros. Sci.*, 2010, **52**, 2891–2896.
47 K. F. Khaled, K. Babic-Samardzija and N. Hackerman, Cobalt(III) complexes of macrocyclic-bidentate type as a new group of corrosion inhibitors for iron in perchloric acid, *Corros. Sci.*, 2006, **48**, 3014–3034.
48 E. A. Noor, Evaluation of inhibitive action of some quaternary N-heterocyclic compounds on the corrosion of Al–Cu alloy in hydrochloric acid, *Mater. Chem. Phys.*, 2009, **114**, 533–541.
49 J. Zhao and G. Chen, The synergistic inhibition effect of oleic-based imidazoline and sodium benzoate on mild steel corrosion in a CO_2-saturated brine solution, *Electrochim. Acta*, 2012, **69**, 247–255.
50 Y. Qiang, S. Fu, S. Zhang, S. Chen and X. Zou, Designing and fabricating of single and double alkyl-chain indazole derivatives self-assembled monolayer for corrosion inhibition of copper, *Corros. Sci.*, 2018, **140**, 111–121.
51 S. Pareek, D. Jain, S. Hussain, A. Biswas, R. Shrivastava, S. K. Parida, H. K. Kisan, H. Lgaz, I. M. Chung and D. Behera, A new insight into corrosion inhibition mechanism of copper in aerated 3.5 wt.% NaCl solution by eco-friendly imidazopyrimidine dye: experimental and theoretical approach, *Chem. Eng. J.*, 2019, **358**, 725–742.
52 S. Masroor, M. Mobin, M. J. Alam and S. Ahmad, The novel iminium surfactant p-benzylidene benzyldodecyl iminium chloride as a corrosion inhibitor for plain carbon steel in 1 M HCl: electrochemical and DFT evaluation, *RSC Adv.*, 2017, **7**(37), 23182–23196.
53 M. T. Alhaffar, S. A. Umoren, I. B. Obot and S. A. Ali, Isoxazolidine derivatives as corrosion inhibitors for low carbon steel in HCl solution: experimental, theoretical and effect of KI studies, *RSC Adv.*, 2018, **8**(4), 1764–1777.
54 X. Yang, F. Li and W. Zhang, 4-(Pyridin-4-yl)thiazol-2-amine as an efficient non-toxic inhibitor for mild steel in hydrochloric acid solutions, *RSC Adv.*, 2019, **9**(19), 10454–10464.
55 F. Yang, Y. Liu, T. Liu, S. Liu and H. Zhao, Aniline trimer-including carboxymethylated β-cyclodextrin as an efficient corrosion inhibitor for Q235 carbon steel in 1 M HCl solution, *RSC Adv.*, 2019, **9**(52), 30249–30258.
56 S. Satpati, S. K. Saha, A. Suhasaria, P. Banerjee and D. Sukul, Adsorption and anti-corrosion characteristics of vanillin Schiff bases on mild steel in 1 M HCl: experimental and theoretical study, *RSC Adv.*, 2020, **10**(16), 9258–9273.
57 T. W. Quadri, L. O. Olasunkanmi, E. D. Akpan, A. Alfantazi, I. B. Obot, C. Verma, A. M. Al-Mohaimeed, E. E. Ebenso and M. A. Quraishi, Chromeno-carbonitriles as corrosion inhibitors for mild steel in acidic solution: electrochemical, surface and computational studies, *RSC Adv.*, 2021, **11**(4), 2462–2475.

Open Access Article. Published on 21 January 2022. Downloaded on 1/21/2026 12:12:41 AM.
This article is licensed under a Creative Commons Attribution-NonCommercial 3.0 Unported Licence.

58 S. Meng, Z. Liu, X. Zhao, B. Fan, H. Liu, M. Guo and H. Hao, Efficient corrosion inhibition by sugarcane purple rind extract for carbon steel in HCl solution: mechanism analyses by experimental and in silico insights, *RSC Adv.*, 2021, **11**(50), 31693–31711.

59 A. Farhadian, A. Rahimi, N. Safaei, A. Shaabani, M. Abdouss and A. Alavi, A theoretical and experimental study of castor oil-based inhibitor for corrosion inhibition of mild steel in acidic medium at elevated temperatures, *Corros. Sci.*, 2020, **175**, 108871.

60 B. Tan, S. Zhang, H. Liu, Y. Qiang and S. Chen, Insights into the inhibition mechanism of three 5-phenyltetrazole derivatives for copper corrosion in sulfuric acid medium via experimental and DFT methods, *J. Taiwan Inst. Chem. Eng.*, 2019, **102**, 424–437.

61 S. Nisha, K. Rajeev, L. Hssane, S. Rachid, C. Ill-Min, K. Sumit and L. Suman, Minified dose of urispas drug as better corrosion constraint for soft steel in sulphuric acid solution, *J. Mol. Liq.*, 2018, **269**, 371–380.

62 Y. Qiang, L. Guo, H. Li and X. Lan, Fabrication of environmentally friendly Losartan potassium film for corrosion inhibition of mild steel in HCl medium, *Chem. Eng. J.*, 2020, **406**, 126863.

63 X. Zheng, S. Zhang, W. Li, L. Yin, J. He and J. Wu, Investigation of1-butyl-3-methyl-1H-benzimidazolium iodide as inhibitor for mild steel insulfuric acid solution, *Corros. Sci.*, 2014, **80**, 383–392.

64 L. Guo, I. B. Obot, X. Zheng, X. Shen, Y. Qiang, S. Kaya and C. Kaya, Theoretical insight into an empirical rule about organic corrosion inhibitors containing nitrogen, oxygen, and sulfur atoms, *Appl. Surf. Sci.*, 2017, **406**, 301–306.

65 L. Guo, S. Zhu, S. Zhang, Q. He and W. Li, Theoretical studies of three triazole derivatives as corrosion inhibitors for mild steel in acidic medium, *Corros. Sci.*, 2014, **87**, 366–375.

 © 2022 The Author(s). Published by the Royal Society of Chemistry